Photoelectron spectroscopy of the negative ion SeO^-

J. V. Coe, J. T. Snodgrass, C. B. Freidhoff, K. M. McHugh, and K. H. Bowen
Department of Chemistry, The Johns Hopkins University, Baltimore, Maryland 21218

(Received 9 August 1985; accepted 10 October 1985)

We have recorded the photoelectron spectrum of SeO^- using a newly constructed negative ion photoelectron spectrometer. The adiabatic electron affinity of SeO is determined to be 1.456 ± 0.020 eV. Values of $\nu_{00}(a\ ^1\Delta - X\ ^3\Sigma^-_{0^+})$ and $\Delta G_{1/2}(a\ ^1\Delta)$ are found to be 5530 ± 200 and $916 \pm 35\ cm^{-1}$, respectively, in substantial accord with previous measurements. The negative ion parameters determined in this work are: $B''_e(SeO^-) = 0.4246 \pm 0.0050\ cm^{-1}$ which leads to $r''_e(SeO^-) = 1.726 \pm 0.010$ Å, $\omega''_e(SeO^-) = 730 \pm 25\ cm^{-1}$, $\omega''_e x''_e(SeO^-) = 2 \pm 4\ cm^{-1}$, and $D_0(SeO^-) = 3.84 \pm 0.09$ eV. In addition, the spectroscopic parameters of SeO^- are compared with those of the electronically analogous negative ions: O_2^-, SO^-, and S_2^-.

I. INTRODUCTION

The selenium monoxide molecule SeO exhibits a rich optical spectrum[1–18] which was first studied as early as 1936. It was, however, 1963 before the first rotational analysis of the SeO spectrum was performed. This was carried out by Barrow and Deutsch[3] for the $B\ ^3\Sigma^- - X\ ^3\Sigma^-$ system in SeO which is analogous to the Schumann–Runge system in O_2. In diatomic molecules composed of group VIB atoms the lowest energy electron configuration gives rise to the molecular states $X\ ^3\Sigma^-$, $a\ ^1\Delta$ and $b\ ^1\Sigma^+$. The forbidden transition $b\ ^1\Sigma^+ - X\ ^3\Sigma^-$ was orginally observed by Azam and Reddy,[8] and has continued to be a subject of study by several investigators.[14–18] The $a\ ^1\Delta$ state of SeO was first observed in the gas phase EPR studies of Carrington, Currie, Levy, and Miller.[19] Later, Reddy and Verma[9] found a band system in the near-infrared and assigned it to the forbidden transition $a\ ^1\Delta - X\ ^3\Sigma^-$.

In other spectroscopic work on SeO, Byfleet, Carrington, and Russell[20] have determined the electric dipole moment of the $a\ ^1\Delta$ state by studying the Stark splitting in its EPR spectrum. Brown, Dumper, and Parent[21] have extended EPR studies on SeO to the millimeter-wave region. Parent and Kuijpers[22] have recorded the millimeter-wave spectrum of SeO at zero field, and Hakuta and Uehara[23] have conducted laser magnetic resonance studies on SeO.

In this work we have applied the technique of negative ion photoelectron (photodetachment) spectroscopy to the study of the negative ion, SeO^-. In the past negative ion photoelectron spectroscopy has also been employed by investigators at the Joint Institute for Laboratory Astrophysics[24–27] to study the electronically analogous negative ions O_2^-, SO^-, and S_2^-. Our work on SeO^- adds a fourth ion to the list of diatomic negative ions composed of group VIB atoms which have been studied by this technique.

Negative ion photoelectron spectroscopy[28] is conducted by crossing a mass selected beam of negative ions with photons of fixed and known energy while the resulting photodetached electrons are subjected to energy analysis. Furthermore, the intersection region is a collision-free and field-free environment. The photodetachment of electrons from molecular negative ions results in rotationally, vibrationally, and electronically excited neutral molecules and in free electrons of the appropriate energy-conserving kinetic energies. Subtraction of the observed electron kinetic energies from the photon energy yields photodetachment transition energies and analysis of such spectra yields electron affinities, vibrational frequencies for the negative ions and their corresponding neutrals, electronic state splittings for the neutrals, and geometric information. Thus, even though these experiments are performed with negative ions, the results pertain to both negative ions and their corresponding neutrals. Here, we report determinations of the electron affinity of SeO, the vibrational frequencies of the $a\ ^1\Delta$ state of SeO and the ground $^2\Pi$ state of SeO^-, the singlet–triplet splitting in SeO, the bond length of SeO^-, and the dissociation energy of SeO^-. The analysis of our SeO^- photoelectron spectrum was facilitated by the availability of extensive spectroscopic information about the neutral SeO radical.

II. EXPERIMENTAL

The apparatus employed in this work is a newly constructed negative ion photoelectron spectrometer which is schematically similar to the instruments of Lineberger[29] and of Ellison.[30] Our spectrometer consists of the following three component systems: a negative ion beam line in which negative ions are formed, transported, and mass selected; a high-power argon ion laser operated intracavity in the ion–photon interaction region; and a magnetically shielded, high resolution hemispherical electron energy analyzer which is located below the plane of the crossed ion and photon beams. Each of these component systems is discussed below and an overview of the apparatus is presented in Fig. 1.

A. Beam line

The beam line originates at the ion source and terminates at the Faraday cup. Its components are housed in four separately pumped vacuum chambers with each chamber downstream from the ion source operating at a successively lower pressure. The two lowest pressure chambers (cham-

 0021-9606/86/020618-08$02.10

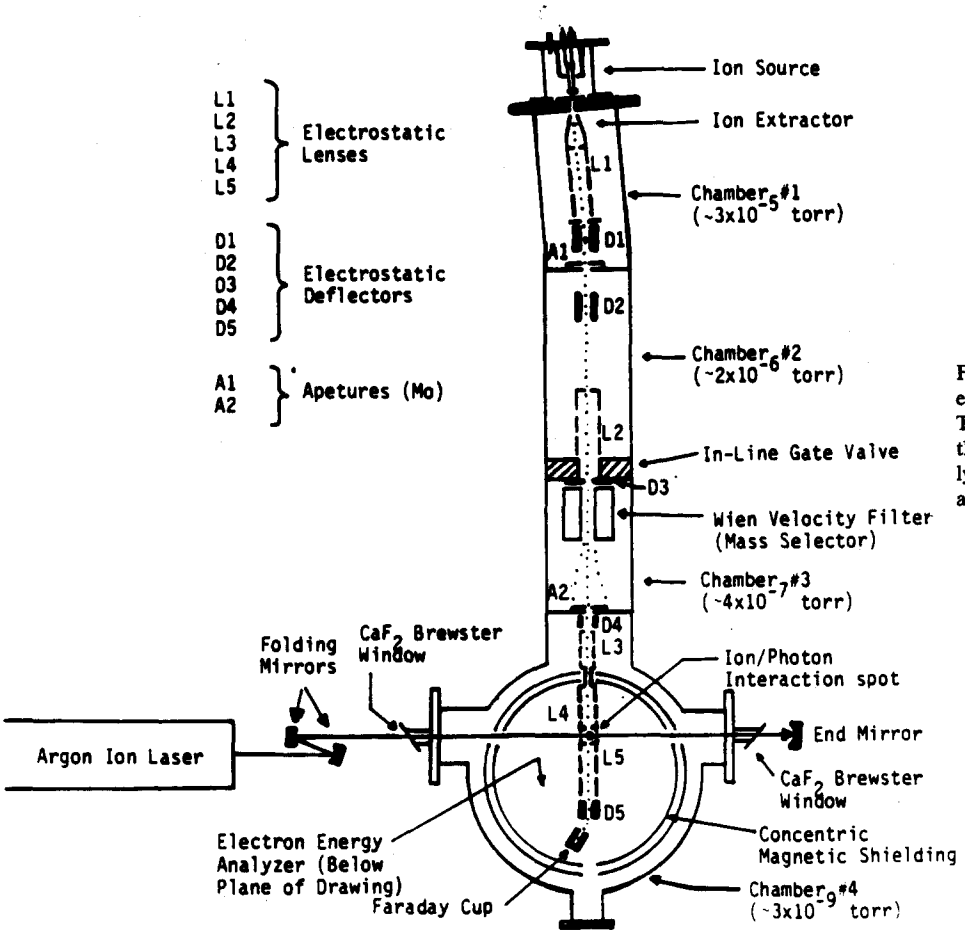

FIG. 1. Diagram of our negative ion photoelectron spectrometer as viewed from above. The negative ion beam, the photon beam, and the acceptance axis of the electron energy analyzer are all oriented at 90° with respect to one another.

bers #3 and #4 in Fig. 1) are pumped by 300 ℓ/s ion pumps while the other two (chambers #1 and #2 in Fig. 1) are, respectively, pumped by 6 and 4 in. oil diffusion pumps with liquid nitrogen cooled baffles.

The first chamber (#1) contains a cylindrical three element electrostatic lens (L1) and horizontal and vertical deflectors (D1). L1 serves not only to focus ions onto the first aperture (A1), but also to extract them from the ion source. All lenses in the ion and electron optical systems were designed using the focal parameter calculations of Harting and Read.[31] The horizontal deflector in D1 deflects the ions exiting L1 by 5° before they impinge on A1 (3 mm in diameter) in order to prevent photons and energetic neutrals from the ion source from reaching the ion–photon interaction region.

Chambers #2 and #3 house the ion optical components for mass analysis. These allow us to "purify" our starting sample of negative ions before photodetachment and thus to obtain interference-free photoelectron spectra of specific negative ions. Chamber #2 contains a pair of corrective deflectors (D2) and a three cylinder electrostatic lens (L2). This lens is operated as an Einzel lens and serves to image the ion beam at the end of the mass selector's drift region with unity magnification. Chamber #3 houses a cooled Colutron 600B Wien filter[32] which acts as a $\mathbf{E}\times\mathbf{B}$ velocity filter. The pumping aperture between chamber #2 and #3 is an externally adjustable vertical slit which may be closed down to obtain more differential pumping or to increase mass resolution by eliminating off-axis ion trajectories in the mass dispersion dimension. The aperture, A2, doubles as the mass spectrometer's output aperture and as the differential pumping hole between chambers #3 and #4. It is 0.2 cm in diameter and 35.5 cm away from the Wien filter's center.

Chamber #4 houses the last ion optical components of the beam line, the ion–photon interaction region, and the electron energy analyzer. Two sequential three cylinder electrostatic lenses image the mass selected ion beam at the ion–photon interaction spot. Beyond the ion–photon interaction region ions are focused and deflected into the Faraday cup detector by a three cylinder lens (L5) and its deflector (D5). We usually observe nanoampere currents of O^-, NO^-, O_2^-, and NO_2^- when N_2O is used as a source gas in our hot-cathode discharge (Branscomb) source.[33]

B. Laser configuration

The laser is a Spectra Physics model 171-18 argon ion laser which is operated intracavity by replacing its front mirror with a set of three highly reflective mirrors to extend the cavity through the ion–photon interaction region in chamber #4. These mirrors were selected so that the waist (<0.04 cm in diameter) of the laser beam occurs in the ion–photon interaction region. The laser is most often operated

on its 488 nm line and achieves a typical power of ~150 circulating watts with a plasma tube discharge current of 35 A. The laser housing is mounted so that the laser's polarization vector makes an angle of ~55° with the electron collection direction. This insures that the angular portion of the differential cross section for photodetachment vanishes so that the measured peak intensities in our spectra are proportional to the total photodetachment cross section.

C. Electron energy analyzer

Figure 2 presents a side view of our hemispherical electron energy analyzer. The entire instrument package is housed in a double layer of annealed magnetic shielding with the inner layer consisting of CoNetic AA and the outer layer being Netic S3-6 shielding.[34] A removable molybdenum aperture near the ion–photon interaction region accepts only a small solid angle (5° semivertical angle) of the photodetached electrons into the electron optics. The analyzer's three main parts: electron injection optics, energy dispersing elements, and electron output optics are discussed below.

The electron injection optics consists of two electrostatic lenses and a pair of deflectors. These input optics are similar to those described by Feigerle.[29] All of the electron lenses are three cylinder lenses made of OFHC copper. The first input lens adds an amount of energy to all electrons such that the electrons of the particular energy being analyzed have 20 times their original kinetic energy. The second input lens is a zoom lens which images the electrons from the first lens at the input plane of the energy dispersing elements with a constant energy. This keeps resolution constant throughout a scan. Both input lenses combine to produce an approximately constant total linear magnification of 1.5 and an angular magnification typically less than 0.5. The last element of the zoom lens contains a pair of deflectors.

The energy dispersing elements are OFHC copper hemispheres. The average radius is 8.890 cm and the gap is 1.905 cm. The radius was chosen as large as was practically feasible with regard to stray magnetic fields so as to maximize sensitivity at a given resolution. The slits are virtual and the elements at the input and output of the hemispheres are at the appropriate Herzog distances so as to terminate the effective dispersing field at the end of the hemispheres.

The output electron optics consist of a single lens with the same object and image distance as the first input lens. There is also a pair of deflectors in the last optical element. The output lens images the hemisphere's output onto a 0.07 cm diameter molybdenum aperture and can accelerate the electrons to 20 times their hemisphere pass energy. Varying the magnification by varying the acceleration allows one to change the resolution without changing the hemisphere pass energy. Electrons which make it through the aperture are accelerated to 300 eV and crash into the front of a Ceratron electron multiplier.

With a pass energy of 5 eV and our present output aperture, the theoretical resolution of our analyzer is ~21 meV (FWHM). In practice we obtain a resolution of ~23 meV (FWHM) on an atomic transition of Se^- with a pass energy of 5 eV. The electron transmission function of the analyzer can be judged from our photoeletron spectrum of O_2^- presented in Fig. 3. This indicates a nearly flat transmission function over most of the spectrum. Furthermore, while electron transmission is expected to fall off for very slow

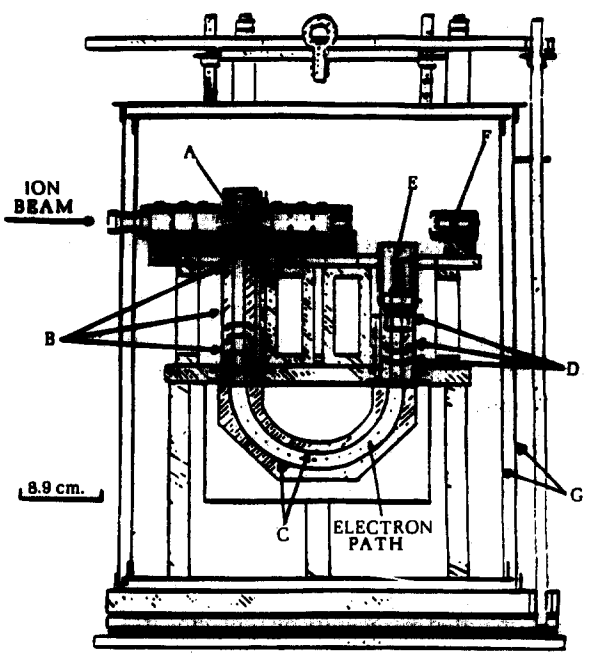

FIG. 2. A side-view diagram of our hemispherical electron energy analyzer. A = ion–photon interaction spot, B = electron input optics, C = hemispheres, D = electron output optics, E = electron multiplier, F = Faraday cup, and G = magnetic shielding.

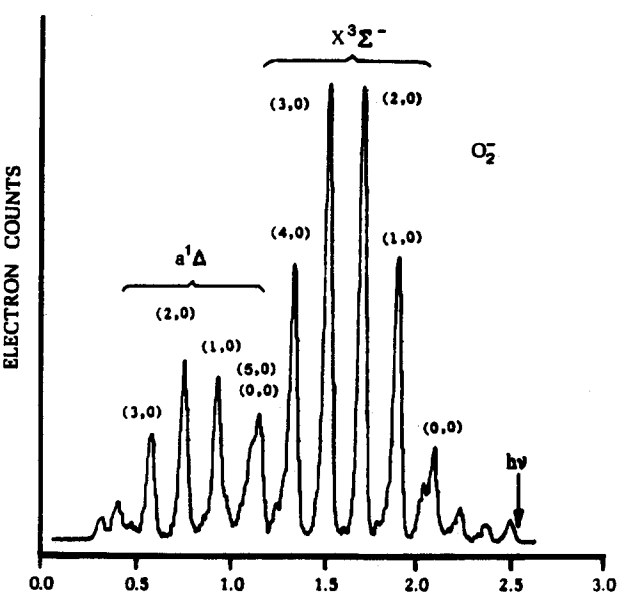

FIG. 3. A photoelectron spectrum of O_2^- recorded on our apparatus with 2.540 eV photons using N_2O in a standard Branscomb source.

electrons, our experience is that the cutoff does not occur until ~0.2 eV.

The overall sensitivity of our apparatus is dependent on several factors beyond those already mentioned, and these include the absolute electron transmission through the analyzer as well as the densities of overlapped ion and photon beams at the interaction spot. The effective overall sensitivity of the apparatus can most easily be assessed by photodetaching O^-. At an instrumental resolution of 30 meV the sensitivity is ~60 cps/nA of O^- per circulating watt of 4880 Å laser power.

D. Production of SeO^-

Selenium monoxide negative ions were produced in a magnetically confined, hot cathode (Branscomb) discharge source[30,33] which we modified for operation at higher temperatures than usual. A typical mass spectrum showing SeO^- is presented in Fig. 4, and mass identifications are confirmed by the observation of selenium isotope patterns. The high temperature modification was implemented by adding a finger to the Branscomb source's quartz housing so that low vapor pressure materials could be heated independently from the rest of the source. Elemental selenium in the finger was maintained at about 350 °C while the rest of the source was maintained at about 225 °C. Roughly 275 mTorr of N_2O was employed as source gas. A thoriated-iridium filament was used and floated at ~150 V negative with respect to the ion source's birth plate. This plate contained a 0.2 cm diameter source aperture and was itself floated at 500 V negative with respect to ground. In general, ~6 A of filament current were sufficient to produce emission currents of 5 to 30 mA which were regulated with a home-built emission current regulator.

III. RESULTS AND ANALYSIS

A. Data for SeO^-

The photoelectron spectrum of SeO^- is presented in Fig. 5. This spectrum was recorded over about an hour with a current of 120×10^{-12} A of SeO^-, and with a channel spacing of 8.4 meV. Since selenium isotopic differences were too small to have an appreciable effect on the observed photoelectron spectrum of SeO^- and since Se^{80} is the most abundant naturally occurring selenium isotope, our SeO^- photoelectron spectra were taken with the mass selector tuned to mass 96. Spectra of O^- were taken immediately before and after every SeO^- spectrum for calibration purposes. At an instrumental resolution of 23 meV the spectrum of O^- appears as a single peak with a large shoulder on the low kinetic energy side and a small shoulder on the high energy side. The peak maximum corresponds to the $O^-(^2P_{3/2})$–$O(^3P_2)$ transition and provides a reference for making relative energy measurements. Photoelectron spectra of O_2^- were also taken on several occasions to check the transmission function of the electron energy analyzer and to provide an energy scale compression factor. This compression factor, which was based on the singlet–triplet splitting in O_2, was typically 0.9992 during these experiments. In order to obtain peak centers, peak heights, and peak areas of optimal

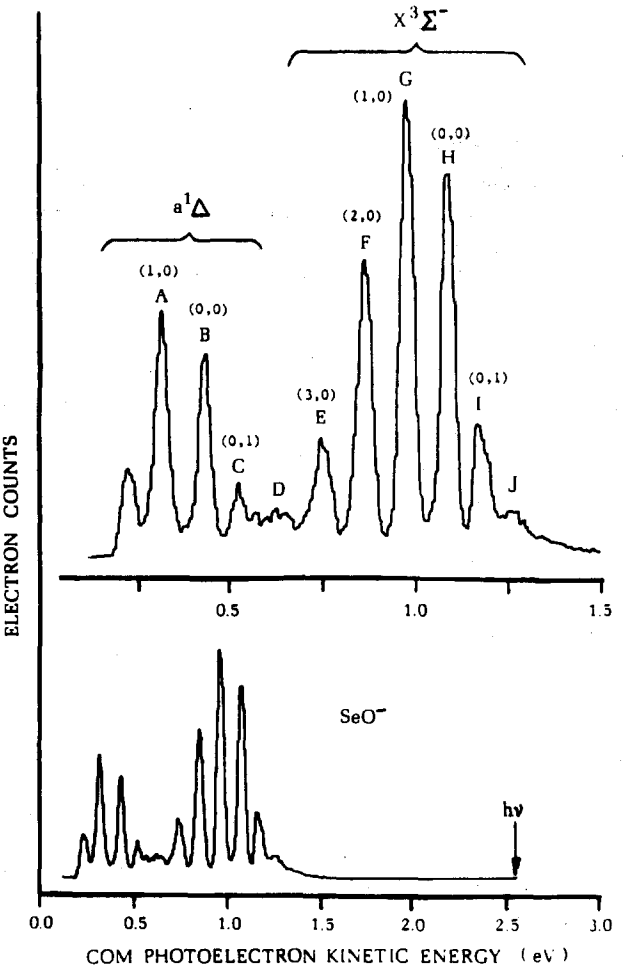

FIG. 5. The photoelectron spectrum of SeO^- recorded on our apparatus with 2.540 eV photons, and presented in terms of center-of-mass (COM) electron kinetic energies. The lower trace shows our entire spectral range while the upper trace is an expanded scale version of the spectral region of interest.

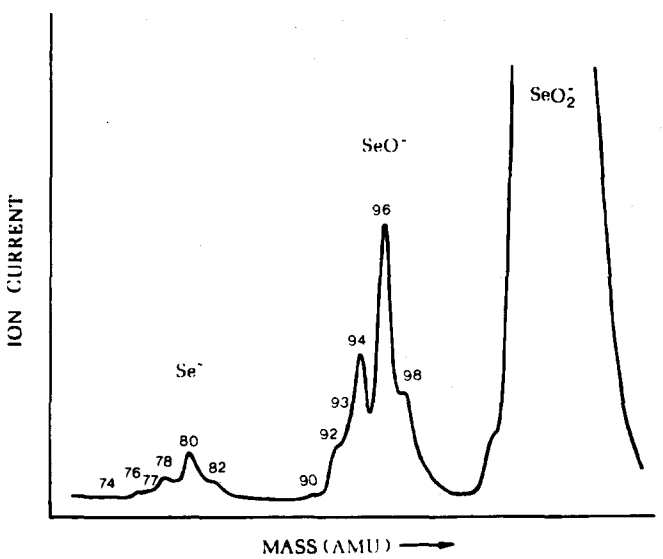

FIG. 4. A negative ion mass spectrum recorded on our apparatus with hot elemental selenium and N_2O gas in our modified Branscomb source.

accuracy, raw data peaks were fit to an asymmetric Gaussian function prior to analysis.

B. Spectral assignment

The photoelectron spectrum of SeO^- bears a strong resemblance to that of SO^-, and an initial guess based simply on inspection of the SO^- spectrum gives an assignment for the SeO^- spectrum that agrees with the following more rigorous approaches. Below, we describe our assignment of the SeO^- spectrum via (a) a consideration of peak spacings and (b) a comparative modeling of the spectrum. The use of isotopic substitution in making an assignment is not helpful in this case because, as mentioned above, the reduced mass of SeO with either oxygen or selenium isotopes does not change enough to move the peaks in the SeO^- photoelectron spectrum by more than a fraction of a meV.

Table I presents the center-of-mass electron kinetic energies of the peak centers as well as peak spacings and our assignments. The first two vibrational states in the ground electronic state of SeO are separated by a $\Delta G_{1/2}$ of 906 cm^{-1}. This is roughly the spacing between peak couples H–G, G–F, and F–E given in Table I and in the SeO^- photoelectron spectrum shown in Fig. 5. While the successive increases in spacing from peak H to E could suggest a negative anharmonicity, they are actually the result of hot band pulling effects as will become clearer in the modeling discussion below. As in O_2 and SO an electron added to SeO goes into an antibonding orbital which implies a longer bond length in the negative ion than in its neutral, and this in turn implies a smaller vibrational frequency in the negative ion. The I,H spacing is significantly smaller than the neutral ground state vibrational spacing. This suggests that peak I and consequently J are due to the negative ion's vibrational spacing, i.e., they are vibrational hot bands. This implication is supported by the observation that while the ratios of peaks H, G, and F remain relatively constant from day to day, peak I may vary by a factor of 2 relative to H, G, or F depending on source conditions. Peaks H, G, F, and E thus define an envelope with a single maximum which implies that they arise from transitions out of the ground vibrational level of the negative ion. By virtue of peak spacings and using the notation (v',v''), we assign peaks H, G, F, and E as the (0,0) (1,0), (2,0), and (3,0) transitions, respectively, from the $^2\Pi$ ground state of SeO^- to the $^3\Sigma^-$ ground state of SeO. In analogy to O_2 and SO one expects the vibrational spacing within the $a\,^1\Delta$ state of SeO to be comparable to that of its $X\,^3\Sigma^-$ ground state. Noticing that the A,B spacing is similar to the G,H spacing and that the B,C spacing is comparable to that previously interpreted as the negative ion's vibrational spacing, leads to an assignment of peaks A, B, and C which is analogous to our interpretation of peaks G, H, and I. We therefore assign peaks A, B, and C as the (1,0), (0,0), and (0,1) transitions from the $^2\Pi$ ground state of SeO^- to the $a\,^1\Delta$ state of SeO.

Although the above interpretation is reasonable, there is still the possibility that peak H is actually the (1,0) peak and that peak I is some unresolved combination of the (0,0) peak and a (1,1) hot band. To investigate this possibility, Franck–Condon factor analyses were performed for the transitions in the $X\,^3\Sigma^-$ envelope of Fig. 5 assuming that peak H was either the (1,0) or the (0,0) transition. An RKR potential was generated for the $X\,^3\Sigma^-$ state of SeO using literature spectorscopic parameters[4] with the $^3\Sigma_1^-$ and $^3\Sigma_{0^+}^-$ states weighted 2:1, respectively. Morse potentials were used for the negative ion. These potentials then become the input for a Franck–Condon program which determined the vibrational energy levels, wave functions, and overlap integrals. The Franck–Condon factors and transition energies were next input into a modeling program which generated spectra which were compared to empirical spectra in a least squares sense. A Boltzmann distribution for the vibrational levels in the negative ion was assumed, and a temperature (800 K) was chosen so as to minimize the sum of the squares of the residuals between the model and empirical spectra. Figure 6(a) presents a best fit assuming that peak H is the (1,0) transition. Under this interpretation most of peak I's area would be due to the (0,0) transition. Peak I should then be taller and shifted more to the high kinetic energy side than it is. Peaks F and E are also poorly fit by this interpretation. Figure 6(b) presents the interpretation of peak H as the (0,0) transition. The fit is very good for peaks H, G, F, and E and much improved for peaks I and J. We attribute the imperfect fit of peaks I and J to the combined effects of considering v'' only up through 3 and a probable deviation in the vibrational population distribution from the Boltzmann distribution which results in a small but noticeable intensity from higher v'' transitions. Figure 6(c) is a plot of the modeled spectra of Fig. 6(b) with all transitions arising from $v'' > 0$ subtracted out. It serves to illustrate how hot bands

TABLE I. Peak locations, spacings, and assignments for our SeO^- photoelectron spectrum.

Peak	COM electron kinetic energy (eV)	Energy (cm^{-1}) from center of peak H	Adjacent spacings (cm^{-1})	Assignment (v',v'')
A	0.300	6230		$a\,^1\Delta(1,0)$
			928	
B	0.415	5310		$a\,^1\Delta(0,0)$
			702	
C	0.502	4610		$a\,^1\Delta(0,1)$
			...	
E	0.726	2800		$X\,^3\Sigma^-(3,0)$
			952	
F	0.844	1850		$X\,^3\Sigma^-(2,0)$
			936	
G	0.960	910		$X\,^3\Sigma^-(1,0)$
			911	
H	1.073	0		$X\,^3\Sigma^-(0,0)$
			734	
I	1.164	730		$X\,^3\Sigma^-(0,1)$

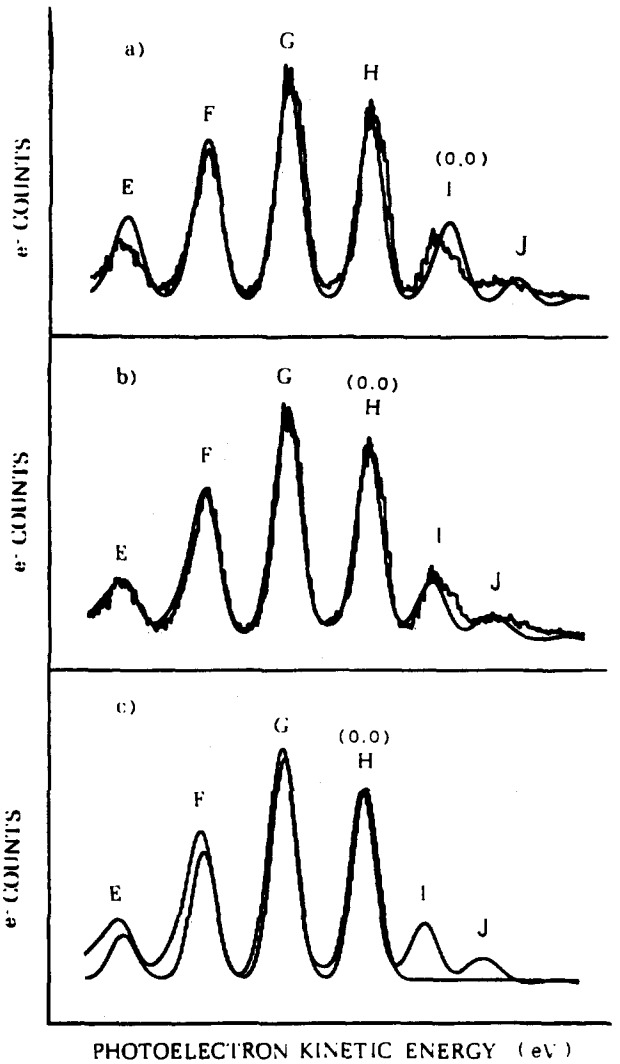

FIG. 6. (a) and (b). Comparisons of the actual SeO^- spectrum with those modeled (smooth curves) on the assumptions: (a) that peak H should be assigned as the (1,0) transition and (b) that peak H should be assigned as the (0,0) transition. (c) A plot of the modeled spectrum in (b) with all transitions arising from $v'' > 0$ substracted out to show the effects of hot band pulling.

can effect peak heights and positions. The negative ion potential parameters determined from the best fit in Fig. 6(b) are $B_e'' = 0.4246 \pm 0.0050$ cm^{-1} leading to a SeO^- bond length, r_e'', of 1.726 ± 0.010 Å, $\omega_e'' = 730 \pm 25$ cm^{-1}, and $\omega_e'' x_e'' = 2 \pm 4$ cm^{-1}. The uncertainty in B_e'' corresponds to the standard deviation in the (1,0)/(0,0) ratio for spectra taken over the course of a week. The uncertainty for ω_e'' also corresponds to the standard deviation in the measured (0,0)–(0,1) spacing for data taken over the course of a week. This method was not particularly sensitive to moderate variations of $\omega_e'' x_e''$ near 0 cm^{-1} but the sum of the squares of the residuals increased quite rapidly for values of $\omega_e'' x_e''$ above 5 cm^{-1}. In summary, the methods of Franck–Condon analysis, peak spacing analysis, and simple analogy with the spectra of SO^- all give the same assignment.

C. Electron affinity of SeO

With a definitive assignment in hand, the transition energy from $v'' = 0$ of the $X\,^2\Pi$ state of SeO^- to $v' = 0$ of the $X\,^3\Sigma^-$ state of SeO may be determined and then corrected for the effects of hot band pulling, spin–spin splitting in the $X\,^3\Sigma^-$ state of SeO, rotational effects, and spin-orbit splitting in the $^2\Pi$ state of SeO^- to yield the adiabatic electron affinity of SeO. Prior to these corrections, however, the adiabatic electron affinity of SeO is given, relative to the O^- calibrant transition, by

$$\text{E.A.}_{\text{SeO}} = \text{E.A.}_{\text{O}} + \gamma(\Omega_{\text{O}} - \Omega_{\text{SeO}}) + mW[(1/M_{\text{O}}) - (1/M_{\text{SeO}})], \quad (1)$$

where E.A._{O} is the electron affinity of atomic oxygen, Ω's are the measured kinetic energy peak positions, γ is the energy scale compression factor, M_{O} and M_{SeO} are the ion masses, m is the mass of an electron, and W is the beam energy. Making these measurements in this manner relative to a calibrant ion with a known electron affinity compensates for any contact potential corrections, and the last term in this equation provides a kinematic correction from measured electron energies to center-of-mass electron kinetic energies. The value of E.A. determined from this equation is 1.467 ± 0.008 eV where the uncertainty is the experimental uncertainty. Hot band pulling effects are negligible for the (0,0) peak as demonstrated by spectral modeling in Fig. 6(c). To correct for the unusually large spin–spin splitting in the neutral ground state, two Gaussians separated by the 165.9 cm^{-1} spin–spin splitting in $X\,^3\Sigma^-$ SeO and weighted 2:1 for the $^3\Sigma_1^-$ and $^3\Sigma_{0^+}^-$ levels, respectively, were added together. Their FWHM's were adjusted so that the FWHM of their sum equaled the empirical FWHM, and then the sum was fit to the functional form of an asymmetric Gaussian. The energy between the peak center and the known $^3\Sigma_{0^+}^-$ position was taken to be the spin–spin splitting correction, and this was -16.1 meV. To make a rotational correction we supposed that the rotational state distribution in the negative ion is adequately approximated by a Boltzmann distribution, and that the rotational temperature of the ion is roughly equal to the vibrational temperature of 800 K obtained during the spectral modeling described above. For this rotational temperature the most abundant rotational state in the negative ion should be $J''(\text{max}) = 25$. An approximate rotational energy correction is then given by[24]

$$(B_e'' - B_e')J''(\text{max})[J''(\text{max}) + 1], \quad (2)$$

where B_e'' and B_e' are the rotational constants of the ground electronic states of SeO^- and SeO, respectively. This correction is -3.8 meV. The spin-orbit splitting correction for the $^2\Pi$ state of SeO^- is more difficult to estimate. Modeling peak H in our spectrum with several different magnitudes of this splitting showed that a spin-orbit splitting of ~ 300 cm^{-1} would cause a visible peak asymmetry that we do not observe. Since the maximum shift in the peak location due to a spin-orbit splitting of between 100 and 300 cm^{-1} occurs in the middle of this range and is ~ 9 meV, we have chosen to employ a spin-orbit correction of $+9$ meV. The combination of all these corrections and uncertainties gives a final

value for the adiabatic electron affinity of SeO of 1.456 ± 0.020 eV.

D. Bond dissociation energy of SeO^-

Given the electron affinities[35] of Se and SeO and the dissociation energy of SeO, the dissociation energy of SeO^- can be calculated from a thermochemical cycle. A variety of dissociation energies for SeO have been quoted in the literature.[36–44] Here, we have chosen to use $D_0(SeO) = 4.40 \pm 0.07$ eV. This is the recently obtained result of Smoes and Drowart[44] who employed a mass spectrometric Knudsen cell method in their thermochemical determination and then corrected their data in light of available spectroscopic data. The use of their best estimate for $D_0(SeO)$ leads to a value for the dissociation energy of SeO^- into the ground states of Se^- and O of 3.84 ± 0.09 eV.

E. The $a\ ^1\Delta$ state of SeO

Since photodetachment transitions involve a change in the total number of electrons in a negative ion–neutral system, any final neutral state is allowed as long as it is energetically accessible with the available photons, and it is due to a single electron, dipole-allowed transition. As a consequence, negative ion photoelectron spectroscopy is an attractive method for measuring the energies of forbidden transitions in neutrals such as singlet–triplet splittings. The $a\ ^1\Delta$–$X\ ^3\Sigma^-$ splitting in SeO is roughly given by the separation between peak H [$X\ ^3\Sigma^-(0,0)$] and peak B [$a\ ^1\Delta(0,0)$] in Fig. 5. Unfortunately, the $a\ ^1\Delta(0,0)$ transition in the SeO^- photoelectron spectrum occurs in the low electron kinetic energy portion of our spectrum where the electron transmission function is of necessity changing. This causes the energy scale compression factor, which is essentially constant over most of the spectrum, to change slightly. To compensate for this effect in the determination of the singlet–triplet splitting, we have measured the location of peak B relative to a nearby transition in our Se^- photoelectron spectrum and the location of peak H relative to the nearby peak of the O^- photoelectron spectrum. After subtracting these transition energies (instead of using the values in Table I) and applying a spin–spin splitting correction for peak H and rotational corrections for both peaks, we find the $a\ ^1\Delta$–$X\ ^3\Sigma^-_{0^+}$ splitting in SeO to be $\nu_{00} = 5530 \pm 200\ cm^{-1}$. Winter, Barnes, Fink, Wildt, and Zabel[17] have set a lower limit for $\nu_{00}(a\ ^1\Delta$–$X\ ^3\Sigma^-)$ of 5238 cm^{-1}. Barrow and Lemanczyk[14] have observed that diatomics with the ground state configuration $...\pi^2$ have a ratio of the term energies of the $a\ ^1\Delta$ and the $b\ ^1\Sigma^+$ states of 0.55 ± 0.05. Since the term energy of $b\ ^1\Sigma^+$ in SeO is known, $T_e(a\ ^1\Delta)$ for SeO is predicted to be $5350 \pm 500\ cm^{-1}$. As mentioned earlier Reddy and Verma[9] have observed a weak emission spectrum from SeO in the near-infrared and assigned it to the $a\ ^1\Delta$–$X\ ^3\Sigma^-_1$ transition. Their $\nu_{00}(a\ ^1\Delta$–$X\ ^3\Sigma^-_1)$ transition energy of 5566.2 cm^{-1} should be less than our $\nu_{00}(a\ ^1\Delta$–$X\ ^3\Sigma^-_{0^+})$ transition energy by the spin–spin splitting (166 cm^{-1}) in $X\ ^3\Sigma^-$ SeO. Thus, the $a\ ^1\Delta$–$X\ ^3\Sigma^-_{0^+}$ transition energy implied by their measurement is 5733 cm^{-1} as compared to ours of $5530 \pm 200\ cm^{-1}$. The spacing between peaks A and B in Fig. 5, which is the energy difference between the $a\ ^1\Delta(1,0)$ and the $a\ ^1\Delta(0,0)$ transitions, gives a value for $\Delta G_{1/2}$ of $916 \pm 35\ cm^{-1}$ after the application of a crude hot band pulling correction. Reddy and Verma, in their analysis of the $a\ ^1\Delta$–$X\ ^3\Sigma^-$ transition, found $\Delta G_{1/2}$ to be 883.3 cm^{-1}.[45] With only the $a\ ^1\Delta(1,0)$ and the $a\ ^1\Delta(0,0)$ transitions available in our spectrum, an anharmoncity constant could not be determined. Also, due to the changing transmission function in this part of the spectrum, no Franck–Condon analysis was attempted on the $a\ ^1\Delta$ system.

IV. SUMMARY OF RESULTS

Directly from the photoelectron spectrum of SeO^- we have determined the adiabatic electron affinity of SeO, the singlet–triplet ($a\ ^1\Delta$–$X\ ^3\Sigma^-$) splitting in SeO, and $\Delta G_{1/2}$ of the $a\ ^1\Delta$ state of SeO. We have found the electron affinity of SeO to be 1.456 ± 0.020 eV. Values of $\nu_{00}(a\ ^1\Delta$–$X\ ^3\Sigma^-)$ and $\Delta G_{1/2}(a\ ^1\Delta)$ have been determined previously.[9] Our values of $\nu_{00}(a\ ^1\Delta$–$X\ ^3\Sigma^-_{0^+})$ and $\Delta G_{1/2}(a\ ^1\Delta)$, which are in rough agreement with previous determinations, are 5530 ± 200 and $916 \pm 35\ cm^{-1}$, respectively. Quantities we have determined for SeO^- which resulted from data reduction are the rotational constant, the bond length, ω_e'',$\omega_e'' x_e''$, and the dissociation energy. Values for these quantities determined in this work are: $B_e''(SeO^-) = 0.4246 \pm 0.0050\ cm^{-1}$, $r_e''(SeO^-) = 1.726 \pm 0.010$ Å, $\omega_e''(SeO^-) = 730 \pm 25\ cm^{-1}$, $\omega_e'' x_e''(SeO^-) = 2 \pm 4\ cm^{-1}$, and $D_0(SeO^-) = 3.84 \pm 0.09$ eV.

TABLE II. Summary of selected spectroscopic parameters for O_2^-, SO^-, SeO^-, and S_2^-.

		$^2\Pi$					
Negative ion, XY^-	E.A.(XY) (eV)	ω_e'' (cm^{-1})	$\omega_e'' x_e''$ (cm^{-1})	B_e'' (cm^{-1})	r_e'' (Å)	D_0 (eV)	Ref.
O_2^-	0.440	1089	12.1	1.17	1.341	4.09	24
SO^-	1.126	895	5	0.643	1.568	4.41	25
SeO^-	1.456	730	2	0.425	1.726	3.84	This work
S_2^-	1.663	524[a]	...	...	...	3.99	27

[a] $\Delta G_{1/2}$.

SeO^- is the fourth diatomic negative ion composed of group VIB atoms to be studied by negative ion photoelectron spectroscopy. It is thus of interest to summarize relevant quantities for these ions. Such a comparative summary is presented in Table II, and it is seen that the SeO^- spectroscopic parameters, including the electron affinity of SeO, conform reasonably well to the trends set by its analogs. Negative ion photoelectron spectroscopy has provided essentially everything that is known about the negative ions and electron affinities of these four molecules and a substantial portion of what is known about the singlet–triplet splitting in their neutrals and the vibrational spacings in their $a\ ^1\Delta$ states.

ACKNOWLEDGMENTS

We thank Paul Dagdigian for making a Franck–Condon analysis program available to us and S. Paddi Reddy for discussions on SeO. We are grateful to Stewart Novick, John Doering, Barney Ellison, Carl Lineberger, Benton Ellis, and Chuck Feigerle for their advice during the apparatus design phase of this work. We would also like to thank Bob Continetti, Terrell Kondziela, Barbara Schwartz, and Paul Lao for their contributions during the building of the apparatus; as well as Joe Walters, Chuck Long, and George Pisiello and his men for superb machine and electronics shop work. This research was supported in part by the Department of Chemistry, by the Research Corporation, and by BRSG Grant S07 RR07041 awarded by the Biomedical Research Support Grant Program, Division of Research Resources, National Institutes of Health. Acknowledgment is also made to the Donors of The Petroleum Research Fund, administered by the American Chemical Society, for partial support of this research.

[1]R. K. Asundi, M. Jan-Khan, and R. Samuel, Proc. R. Soc. London **157**, 28 (1936).
[2]C. Shin-Piaw, Ann. Phys. (Paris) **10**, 173 (1938).
[3]R. F. Barrow and E. W. Deutsch, Proc. Phys. Soc. **82**, 548 (1963).
[4]K. P. Huber and G. Herzberg, *Molecular Spectra and Molecular Structure IV. Constants of Diatomic Molecules* (Van Nostrand–Reinhold, New York, 1979).
[5]P. B. V. Haranath, J. Mol. Spectrosc. **13**, 168 (1964).
[6]P. B. V. Haranath, Ind. J. Pure Appl. Phys. **3**, 75 (1965).
[7]V. S. Kushawaha and C. M. Pathak, Sprectrosc. Lett. **5**, 393 (1972).
[8]M. Azam and S. P. Reddy, Can. J. Phys. **51**, 2166 (1973).
[9]S. P. Reddy and K. K. Verma, J. Mol. Spectrosc. **84**, 89 (1980).
[10]K. K. Verma, M. Azam, and S. P. Reddy, J. Mol. Spectrosc. **65**, 289 (1977).
[11]K. K. Verma, M. Azam, and S. P. Reddy, J. Mol. Spectrosc. **58**, 367 (1975).
[12]S. P. Reddy and M. Azam, J. Mol. Spectrosc. **49**, 461 (1974).
[13]W. E. McDermott and D. J. Benard, Chem. Phys. Lett. **64**, 60 (1979).
[14]R. F. Barrow and R. Z. Lemanczyk, Can. J. Phys. **53**, 553 (1975).
[15]K. K. Verma and S. P. Reddy, J. Mol. Spectrosc. **67**, 360 (1977).
[16]P. Kristiansen, Can. J. Phys. **56**, 1399 (1978).
[17]R. Winter, I. Barnes, E. H. Fink, J. Wildt, and F. Zabel, Chem. Phys. Lett. **73**, 297 (1980).
[18]M. Bielefeld, G. Elfers, E. H. Fink, H. Kruse, J. Wildt, R. Winter, and F. Zabel, J. Photochem. **25**, 419 (1984).
[19]A. Carrington, G. N. Currie, D. H. Levy, and T. A. Miller, Mol. Phys. **17**, 535 (1969).
[20]C. R. Byfleet, A. Carrington, and D. K. Russell, Mol. Phys. **20**, 271 (1971).
[21]J. M. Brown, K. Dumper, and C. R. Parent, Mol. Phys. **36**, 1149 (1978).
[22]C. R. Parent and P. J. M. Kuijpers, Chem. Phys. **40**, 425 (1979).
[23]K. Hakuta and H. Uehara, J. Mol. Spectrosc. **85**, 97 (1981).
[24]R. J. Celotta, R. A. Bennett, J. L. Hall, M. W. Siegel, and J. Levine, Phys. Rev. A. **6**, 631 (1972).
[25]R. A. Bennett, Ph. D. dissertation, University of Colorado, 1972.
[26]W. C. Lineberger, in *Laser Spectroscopy*, edited by R. Brewer and A. Morradian (Plenum, New York, 1974), pp. 581–595.
[27]R. J. Celotta, R. A. Bennett, and J. L. Hall, J. Chem. Phys. **60**, 1740 (1974).
[28]R. R. Corderman and W. C. Lineberger, Annu. Rev. Phys. Chem. **30**, 347 (1979).
[29]C. S. Feigerle, Ph.D. dissertation, University of Colorado, 1983.
[30]H. B. Ellis, Jr. and G. B. Ellison, J. Chem. Phys. **78**, 6541 (1983).
[31]E. Harting and F. H. Read, *Electrostatic Lenses* (Elsevier, Amsterdam, 1976).
[32]Purchased from Lars Wälin of Colutron Corporation in Boulder, Colorado.
[33]L. M. Branscomb, D. S. Burch, S. J. Smith, and S. Geltman, Phys. Rev. **111**, 504 (1958).
[34]CoNetic AA and Netic S3-6 are the trade names of Perfection Mica Co. of Bensenville, Illinois for high premeability, low saturation and high saturation, low permeability magnetic shielding, respectively.
[35]H. Hotop, T. A. Patterson, and W. C. Lineberger, Phys. Rev. A **8**, 762 (1973).
[36]J. Drowart and P. Goldfinger, Q. Rev. Chem. Soc. **20**, 545 (1966).
[37]G. DeMaria, Corsi Semin. Chim. **6**, 15 (1967).
[38]S. V. J. Lakshman, T. V. R. Rao, and G. T. Naidu, Ind. J. Pure Appl. Phys. **15**, 834 (1977).
[39]A. G. Gaydon, *Dissociation Energies* (Chapman and Hall, London, 1968).
[40]B. Rosen, *Spectroscopic Data Relative to Diatomic Molecules* (Pergamon, Oxford, 1970).
[41]C. Glidewell, Inorg. Chim. Acta **24**, 149 (1977).
[42]J. B. Pedley and E. M. Marshall, J. Phys. Chem. Ref. Data **12**, 967 (1983).
[43]A. J. Sauval and J. B. Tatum, Astrophys. J. Suppl. Ser. **56**, 193 (1984).
[44]S. Smoes and J. Drowart, J. Chem. Soc. Faraday Trans 2 **80**, 1171 (1984).
[45]The value of $\Delta G_{1/2}$ given in Ref. 9 is a typographical error and should read 883.3 cm^{-1}. S. P. Reddy (private communication).